

## Correlation between magnetism and structure in ultrathin Fe/Cu<sub>3</sub>Au(001) films

F. Bisio,\* S. Terreni, M. Canepa, and L. Mattera

CNR-INFM, Unità di Genova, Dipartimento di Fisica, Università di Genova, via Dodecaneso 33, I-16146 Genova, Italy

(Received 6 May 2005; revised manuscript received 21 September 2005; published 10 November 2005)

We have studied the correlation between the magnetic properties and the structure of ultrathin ferromagnetic Fe/Cu<sub>3</sub>Au(001) films for thicknesses up to 15 Å. We have found that two different face centered tetragonal structural phases coexist within the film in the thickness range 5–15 Å. The coexistence of the two structural phases induces an anomalous thickness dependence of the Curie temperature of the films. We ascribe this thickness dependence to a difference in the exchange coupling between the two phases. The irreversible modifications of the magnetic properties of the films after a mild thermal treatment are discussed on the basis of the corresponding changes of the structure and the morphology.

DOI: [10.1103/PhysRevB.72.174413](https://doi.org/10.1103/PhysRevB.72.174413)

PACS number(s): 75.70.Rf, 68.55.–a

### I. INTRODUCTION

The Cu<sub>3</sub>Au(001) surface has been widely employed as a substrate for the epitaxial growth of Fe films.<sup>1–10</sup> Interest in this system was mostly motivated by the possibility of growing Fe films which, in the ultrathin limit, could exhibit fcc structure and ferromagnetic (FM) order.

The comparison with the most popular Fe/Cu(001) system has allowed verification of the vast amount of theoretical predictions about the magnetic ground state of fcc iron and its dependence on the lattice constant.<sup>11–13</sup> However, a recent study of Fe/Cu(001) ultrathin films (2–4 ML), pointed out that the compressive strain that Cu exerts upon Fe pushes the films into a strained body centered cubic (bcc) structure, thereby questioning the existence itself of ferromagnetic Fe in fcc structure.<sup>14</sup>

In this respect, since the lattice constant of Cu<sub>3</sub>Au ( $a = 2.65$  Å) is larger than the one of Cu(001) ( $a = 2.55$  Å), we expect a decrease of the compressive strain on the Fe films with respect to the Cu(001). This decrease should reduce the tendency to the strain-driven formation of the bcc-like nanocrystal observed in Fe/Cu, and support the growth of fcc Fe. The fcc Fe with the Cu<sub>3</sub>Au lattice constant is predicted to be FM ordered.<sup>11–13</sup>

The structure of ultrathin films of Fe/Cu<sub>3</sub>Au(001), and the formation of a fcc phase in the early stages of growth have been, for a long time, a subject of debate. Some investigations<sup>1,2,15</sup> claimed the occurrence of a fcc Fe phase in the early stages of growth, followed by the nucleation of a body centered tetragonal (bct) structure.<sup>2,15</sup> Instead, in a subsequent experiment<sup>4</sup> the Fe structure was assigned to a strained bct phase.

More recent investigations<sup>5</sup> revealed the presence of a complex scenario in which different structural phases of Fe were found to coexist for films deposited at RT. An almost undistorted face centered tetragonal (fct) structure was found for coverage  $\approx 3$  Å. The coexistence of this phase with a second fct phase was found for thicknesses larger than  $\approx 6$  Å. The nucleation of the bct phase took place around 15 Å.

The somehow contradictory results reported in the literature are due to the inherent metastability of this system. This

conclusion is supported by the observation for Fe/Cu<sub>3</sub>Au films of a striking temperature dependence of the structure of the whole film.<sup>8</sup>

Despite this general controversy about the structure, an agreement about the magnetic properties has been reached. It is well established that ultrathin Fe/Cu<sub>3</sub>Au(001) films are ferromagnetic,<sup>1–3,6</sup> in agreement with the theoretical predictions.<sup>11–13</sup> The FM behavior is observed irrespective of the details of the sample preparation procedure, and in all cases Fe/Cu<sub>3</sub>Au(001) films were found to be uniformly magnetized. In the early stages of growth, films exhibit out-of-plane easy axis of magnetization, which eventually switches to in-plane via a spin reorientation transition (SRT).<sup>2,3,6</sup>

The authors of Ref. 2 found a correlation between the nucleation of the bct phase and the occurrence of the SRT. However, a subsequent study<sup>3</sup> did not find any evidence for the fct  $\rightarrow$  bct transition and did not observe any correlation between a change in the film structure and the occurrence of the SRT. Recent theoretical work pointed out the crucial role of Au segregation in determining the SRT thickness.<sup>16</sup>

The purpose of this paper is to pursue further the investigation of the correlation between the structure and the magnetism of Fe/Cu<sub>3</sub>Au(001) films. Backed by a reliable structural analysis, we have characterized the magnetic properties of Fe/Cu<sub>3</sub>Au(001) films. We focus our attention on the whole thickness range for which the coexistence of two fct phases was observed.<sup>5</sup> The upper thickness limit is set by the nucleation of the bct phase. We observe that the coexistence of fct structures affects the magnetic properties of the films; the thickness dependence of the Curie temperature  $T_C$  clearly reflects the different magnetic properties of the two fct phases.

### II. EXPERIMENT

Experiments have been performed in an UHV chamber with base pressure below  $1 \times 10^{-10}$  mbars equipped with facilities for preparation and analysis of ultrathin magnetic films.<sup>8,17</sup> The chamber features low energy electron diffraction (LEED), Auger electron spectroscopy (AES), and the magneto-optical Kerr effect (MOKE) in polar and longitudinal configuration. Magnetic fields up to 1 KOe are provided

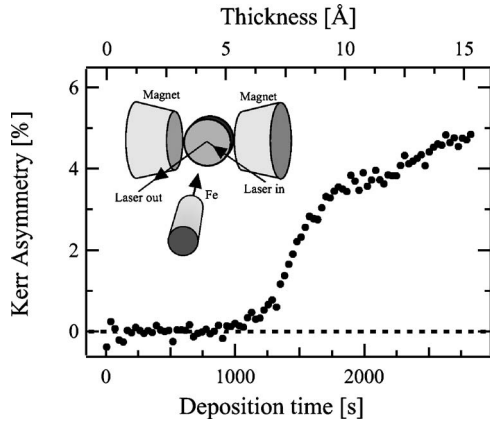


FIG. 1. Longitudinal Kerr asymmetry  $A_K$  for the growth of Fe at 300 K on clean  $\text{Cu}_3\text{Au}(001)$  as a function of the deposition time (bottom axis) and thickness (top axis). The onset of the Kerr signal marks the thickness for which the Curie temperature of the system exceeds the deposition temperature (300 K). See text for details of the thickness calibration procedure. The arrangement of sample, electromagnet, and evaporator for the longitudinal MOKE is depicted in the inset.

by an UHV mounted soft-iron electromagnet. The arrangement of the components within the chamber (Fig. 1) is such that it allows MOKE measurement in either polar or longitudinal configuration to be performed in real time during film growth.

A clean and ordered  $\text{Cu}_3\text{Au}(001)$  surface was prepared according to well-established procedures.<sup>18,19</sup> After cleaning, the substrate surface exhibited the  $c(2 \times 2)$  reconstruction typical of the Cu-Au termination of the so-called  $L1_2$  bulk structure, with sharp diffraction spots, indicative of structural and chemical order. The preparation procedure employed should ensure that the surface is composed mainly by Au-rich terraces.<sup>19,20</sup> However, no influence of the terrace type on the structure and morphology of the Fe films has been reported.<sup>15</sup> Fe has been deposited from the tip of a high purity wire. Pressure rise in the chamber during evaporation was typically less than  $2 \times 10^{-10}$  mbars. We stress that all the films have been systematically deposited with the substrate held at 300 K. This has been done in order to be consistent with the experimental procedure of Ref. 5. In fact, it has been observed that a different substrate temperature during the growth leads to a different thickness dependence of the structure<sup>8</sup> and of the magnetism<sup>2</sup> of the films.

In order to obtain excellent reproducibility of film thickness we rely upon the possibility of measuring the MOKE in real time during the deposition of Fe. We define the Kerr asymmetry as  $A_K = (I_{\uparrow} - I_{\downarrow}) / (I_{\uparrow} + I_{\downarrow})$ , where  $I_{\uparrow(\downarrow)}$  is the light intensity detected after the analyzer for opposite sample magnetization directions. As an example, in Fig. 1 we report  $A_K$  at saturation in longitudinal configuration as a function of time during the deposition of Fe onto a clean  $\text{Cu}_3\text{Au}(001)$  surface at 300 K. The experimental procedure employed to obtain this curve is as follows: the sample is magnetized at saturation in a given direction applying a magnetic field of 50 Oe and kept at saturation for a time sufficient to measure  $I_{\uparrow}$  with the desired accuracy. The polarity of the field is then

reversed and  $I_{\downarrow}$  is measured. Meanwhile Fe is deposited from the evaporator. The procedure is then iterated to obtain the  $A_K$  vs thickness curve. One can alternatively measure  $A_K$  at remanence by saturating the sample in opposite directions, setting the external field to zero and successively measuring  $I_{\uparrow(\downarrow)}$ . In the curve of Fig. 1 we easily observe thickness dependent features such as the steep onset of the magnetic signal around 1400 sec of deposition. We therefore employ the thickness dependence of  $A_K$  as a calibration curve to obtain reproducible thickness across different depositions. Due to the high signal to noise ratio and the excellent stability of the evaporation rate, the reproducibility in achieving the same nominal thickness in independent depositions is better than  $\pm 5\%$ .

The absolute calibration of the thickness relies upon the combination of several methods. Estimates of the amount of Fe are given by means of a quartz microbalance reading and quantitative AES measurements. Estimates are cross-checked by careful comparison of our thickness dependent magnetic (or structural) features with the corresponding data reported in the literature. Due to the discrepancies still present between different investigations, the *absolute* thickness reading suffers large uncertainties, which can be quantified as  $\pm 15\%$ . We notice that the absolute uncertainty in the thickness does not by any means affect our capability of obtaining any desired *nominal* thickness with the above mentioned reproducibility of  $\pm 5\%$ .

We have characterized the Fe/ $\text{Cu}_3\text{Au}(001)$  films in the thickness range up to 15 Å. We noticed that strong modifications of the structure, morphology, and magnetic properties take place upon mild annealing of the films.<sup>9,17</sup> Therefore we exploited such changes in order to gain insight into the correlation between the film structure and its magnetism. The typical measurement scheme is as follows. Films of the desired thickness are deposited onto the substrate held at 300 K; immediately after deposition all the films are cooled at 180 K. We refer to this state as the “as-deposited” state. At this temperature, LEED spot profiles and AES spectra are measured. Following these measurements, the films are slowly annealed ( $dT/dt \sim 2$  K/min) to a maximum temperature  $T_{max}$ . After Ref. 8,  $T_{max}$  is set to 365 K for thicknesses below 12.5 Å and 395 K for larger thicknesses. During the annealing the dependence of  $A_K$  at remanence upon temperature is measured, thus yielding the Curie temperature  $T_C$ . After reaching  $T_{max}$ , the films are rapidly cooled to 180 K. We refer to this state as the “annealed” state. Spot profiles and AES spectra are measured again at 180 K. The films are then annealed again while measuring  $A_K$ , in order to yield the critical temperature  $T_C$  in the annealed state. The LEED spot profiles are measured along the high symmetry crystallographic directions and AES spectra include low energy and high energy Auger lines of Fe, Cu, and Au.

### III. RESULTS

#### A. Structure

In Fig. 2 we report the LEED measurements (electron energy  $E=58.1$  eV) of the surface (11) diffraction spot as a

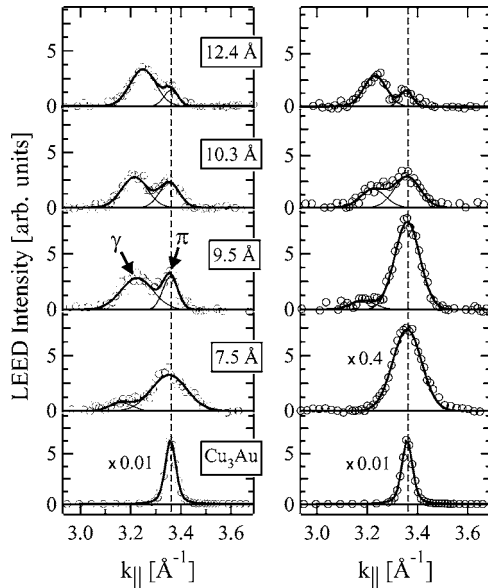


FIG. 2. LEED spot profiles of the (11) surface diffraction spot as a function of Fe thickness (electron energy is 58.1 eV). The left column displays the spot profiles measured for films in the as-deposited state. The right column displays the same reciprocal space region measured for films in the annealed state. All the films have been deposited at 300 K. All the profiles have been measured at 180 K.

function of the Fe thickness. In the left column we report the measurements of the as-deposited state, while the data relative to the annealed state are shown in the right column. In order to focus attention upon the structure, we have subtracted from the data (with the exception of the clean substrate profile) a smooth Lorentzian background originating from the large number of defects accumulated during the growth.

The clean substrate diffraction spot, corresponding to 2.65 Å real space periodicity, is reported in the bottom panel for reference purposes. The LEED patterns substantially evolve as a function of Fe thickness. At coverages smaller than 5.5 Å the (11) spot is composed of a single peak located at the same reciprocal space position as the substrate peak (pseudomorphic peak, referred to as  $\pi$  in the following). At a thickness of 5.5 Å, beside the  $\pi$  peak, a second peak, which we label  $\gamma$ , appears at smaller  $k_{\parallel}$ . The  $\gamma$  peak gradually evolves from a little more than a shoulder of the  $\pi$  peak until it becomes the only detectable contribution at a thickness of 13 Å. Its position corresponds to a real space periodicity between 2.78 and 2.74 Å. We still observe the  $\pi$  peak up to a film thickness of 12.4 Å. Since the electron mean free path in Fe deduced from the attenuation of the substrate Cu 60 eV Auger line is much smaller ( $< 5$  Å), we conclude that  $\pi$  and  $\gamma$  phases coexist in the film for coverages above 5.5 Å, in agreement with Ref. 5.

The profiles reported in the right panel of Fig. 2 clearly show that even a mild annealing heavily affects the film diffraction pattern. The modifications are large on the films less than 9.5 Å thick, and gradually become less relevant with increasing thickness. For film thickness up to 7.5 Å we witness the complete disappearance of the  $\gamma$  peak upon anneal-

ing at 365 K. At 9.5 Å thickness the  $\gamma$  peak persists after the annealing, but its intensity is strongly reduced. At 10.3 Å the effect of annealing is only to shift the relative balance of the  $\pi$  and  $\gamma$  peaks in slight favor of  $\pi$ , while at 12.4 Å and above almost no effect is observable. Overall, the diffraction peaks become broader after the annealing.

We have measured and analyzed the thickness dependence of the intensity of the low energy lines of Cu (58 and 60 eV), Au (66 and 69 eV), and Fe (47 eV). For as-deposited films, the intensity of the Cu lines quickly decreases for increasing Fe thickness, dropping below our experimental sensitivity at a coverage above 5.5 Å. The Au lines reduce their intensities up to reach approximately 10% of the clean surface value at 5.5 Å thickness, and thereafter remain constant for increasing coverage. Comparing our findings with previous investigations,<sup>3,21</sup> we can conclude that the relative amount of Cu interdiffused or segregated in the film is below 1%, whereas approximately  $0.2 \pm 0.1$  monolayers of Au are segregated at the surface.

After the annealing, relevant changes in the AES spectra are observed as well. Below 9.5 Å we observe an increase of the intensity of the Au low energy Auger lines, accompanied by the reappearing of the Cu lines. The intensity of the Cu lines after the annealing is approximately  $10^2$  times smaller with respect to the clean substrate. For films thicker than 9.5 Å only a very slight increase of the low energy Au Auger line is seen, and the Cu contribution remains undetectable even after the annealing. The irreversible modifications take place upon the *first* annealing only. Upon additional thermal treatments a completely reversible behavior is observed.

The behavior of the Cu AES line, together with the observed broadening of the LEED peaks in the annealed state, suggest that the annealing induces the formation of Fe mounds, in analogy with other Fe thin film systems.<sup>22,23</sup> In fact, the reappearance of a Cu AES signal cannot be due to interdiffusion or segregation which takes place only at a temperature much higher than  $T_{max}$ .<sup>3</sup> Instead, the formation of the mounds depletes the interstitial regions in which the local thickness becomes smaller than the electron mean free path, allowing substrate contributions to AES to be detected. Due to the very low intensity of the Cu Auger line after the annealing, we consider unlikely the formation of disconnected Fe mounds separated by uncovered substrate, although we cannot exclude that limited areas of uncovered substrate may exist. From the broadening of the LEED peaks we deduce a mean mound size of about 10 nm.

## B. Magnetism

The complexity of the structural and morphological properties of the Fe/Cu<sub>3</sub>Au(001) films affects their magnetic properties as well. We have first characterized the magnetic anisotropy of the films by measuring MOKE in polar and longitudinal configuration. We have observed that the as-deposited films with thicknesses between 3 and 5.5 Å are ferromagnetically ordered and exhibit out-of-plane easy axis of magnetization, while the films with thicknesses larger than 7 Å have in-plane easy axis of magnetization. Thus a SRT has taken place at a thickness between 5.5 and 7 Å. We

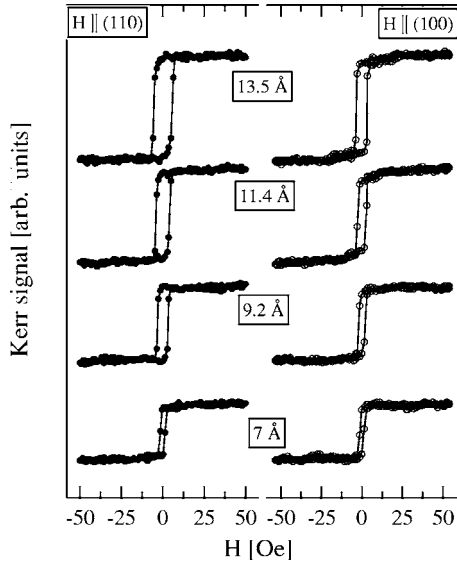


FIG. 3. The longitudinal MOKE hysteresis loops for Fe films of various thicknesses in the as-deposited state. The left part of the graph displays loops measured with external field  $\mathbf{H} \parallel (110)$  direction, while loops measured with  $\mathbf{H} \parallel (100)$  are reported in the right part of the graph.

observe therefore, in contrast to a previous investigation,<sup>2</sup> that no correlation between the SRT and a structural transformation is present. There is no change in the orientation of the easy axis of magnetization after the annealing.

In the following, we will focus our attention on the magnetic properties of the in-plane magnetized films, in the thickness range for which the phase coexistence is demonstrated by the structure data. Longitudinal MOKE hysteresis loops measured for various Fe thickness within such a range are reported in Fig. 3. In all the following measurements the saturating external field is set parallel to the fcc (110) direction, for which the longitudinal MOKE hysteresis loops are square and show full remanence. The hysteresis loops in the annealed state have sigmoidal shape, but still exhibit a full remanence.

In Fig. 4 we report the temperature dependence of the longitudinal Kerr asymmetry at remanence in the as-deposited state (upper panel) and in the annealed state (lower panel) for films of various thicknesses. We clearly observe that striking differences in the magnetic properties of the annealed films with respect to the as-deposited state are present. Analogously to the structure, large irreversible modifications have taken place. We will focus our attention on the modification of the critical temperature of the films and of their MOKE signal.

From the data in Fig. 4 we can extract the Curie temperature  $T_C$  and the Kerr asymmetry extrapolated at  $T=0$  K [ $A_K(0)$ ] by fitting the experimental  $A_K(T)$  curves according to the scaling law

$$A_K(T) = A_K(0)(1 - T/T_C)^\beta. \quad (1)$$

The best fits to the data are reported as solid lines on the graph. We employ a fitting procedure analogous to the one described in Ref. 24, according to which  $T_C$  is found by

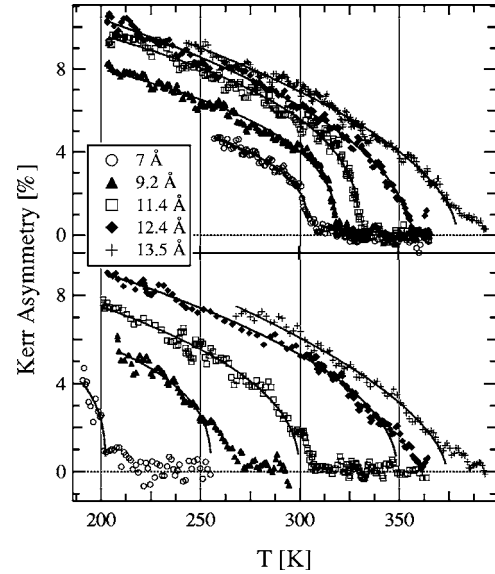


FIG. 4. The experimental temperature dependence of the longitudinal Kerr asymmetry  $A_K$  (symbols) for selected Fe thickness. The top panel displays the data recorded for as-deposited films. The bottom panel shows the corresponding curves measured in the annealed states. The solid lines are the best fit to the experimental curves according to Eq. (1).

maximizing the temperature range over which the data points in a  $\log_{10} M$  vs  $\log_{10}(1 - T/T_C)$  representation form a straight line. Such a procedure allows us to minimize systematic errors arising from the possible presence of magnetization tails above the Curie temperature. Its applicability must be carefully considered when such magnetization tails above  $T_C$  extend for more than a few kelvins. Experimentally (see Fig. 4), we notice that such tails are present for the 13.5 Å thick as-deposited film and for all the films in the annealed state. This effect is likely due to the above mentioned formation of Fe mounds during epitaxy<sup>25</sup> and after annealing.<sup>22,23</sup> The presence of such imperfections in the sample affects the magnetic properties in the vicinity of the phase transition via finite size effects. In the presence of such large tails, we still employ the above mentioned fitting procedure, keeping in mind that the values of  $T_C$  and  $\beta$  for these films might suffer from a larger uncertainty, which, however, does not affect our results.

The best fit parameters  $A_K(0)$  and  $T_C$  are reported in Fig. 5. The value of  $A_K(0)$  for as-deposited films (closed triangles) increases linearly with thickness, indicative of a uniformly magnetized film. The  $A_K(0)$  for annealed films (open triangles) follows a straight line only for a thickness larger than 10 Å, but deviate from the linear thickness dependence for lower coverage. If one compares the annealed  $A_K(0)$  values point by point with the corresponding as-deposited values, it appears that, for thicknesses larger than 10 Å,  $A_K(0)$  has decreased by an amount roughly independent of thickness, whereas no definite behavior is resolvable for the lower thickness.

Coming to the bottom panel, we observe that for as-deposited films,  $T_C$  initially rises very slowly, going from  $T_C=304$  K for the 7 Å film to  $T_C=330$  K for 11.4 Å. There-

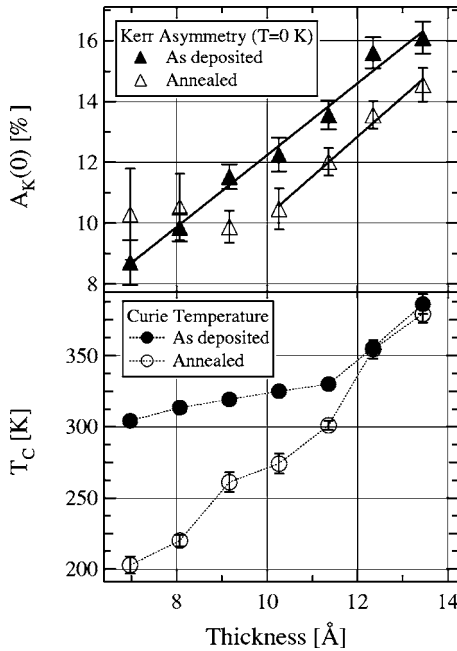


FIG. 5. Upper panel: thickness dependence of the Kerr asymmetry  $A_K(0)$  extrapolated at  $T=0$  K for as-deposited films (closed triangles) and annealed films (open triangles). The solid line is a linear fit to the  $A_K(0)$  for as-deposited films. Bottom panel: thickness dependence of the critical temperature  $T_C$  for as-deposited films (closed circles) and annealed films (open circles). Data were extracted from the best fits of experimental  $A_K(T)$  according to Eq. (1). The dotted lines are only guides to the eye.

after, it steeply increases for larger thicknesses, becoming larger than 380 K at a thickness of 13.5 Å. At coverages of 14.5 Å for which we do not observe yet the nucleation of a bct phase, a magnetic signal remains clearly observable up to a temperature  $T > 480$  K.

For the annealed films we observe a considerable thickness-dependent reduction of the value of  $T_C$  with respect to the as-deposited case, out of the experimental uncertainty. For the 7 Å film,  $T_C$  is reduced by almost 100 K. The amount by which  $T_C$  is reduced after the annealing then decreases with increasing thickness and becomes compatible with zero for the 12.4 and 13.5 Å thick films.

We notice that the critical exponent  $\beta$  extracted from the best fits is found in between the three-dimensional (3D)-Ising (0.325) and 3D-Heisenberg (0.37) values for films with thickness below 12 Å. The  $\beta$  apparently tends to become larger for larger thickness. Its increase occurs for both as-deposited and annealed films, and is obtained irrespective of the temperature range employed for fitting the critical behavior. However, a large value of  $\beta$  (approaching 0.5), is clearly unphysical for our system. This increase might be due to the uncertainties in the determination of  $\beta$  introduced by the large magnetization tails above  $T_C$ , and by the occurrence of a modification of the system that causes a deviation of the temperature dependence of the magnetization from Eq. (1). We will address this point in the framework of discussion.

In analogy with the structural measurements, we observe that the irreversible modifications of the magnetic properties occur upon the first annealing only. Perfect reversibility is then observed for subsequent thermal cycles.

## IV. DISCUSSION

### A. Structure

The evolution of the in-plane structure of the as-deposited films as a function of thickness agrees very well with the findings of Ref. 5. We clearly observe the nucleation and development of a structural phase ( $\gamma$ ) that decreases the elastic strain by enlarging its lattice constant towards the equilibrium Fe value. Furthermore, from our LEED data we conclude that for thicknesses between 13 Å and the maximum of our investigated range (15 Å) all the topmost surface layers possess the  $\gamma$  phase coordination. We stress that, according to our estimates of the electron mean free path, our LEED measurements probe the topmost 2–3 layers of the film and weigh the relative amount of  $\pi$  and  $\gamma$  phase according to their presence in the topmost layers. The  $\pi$  and  $\gamma$  phases, after Ref. 5, are both of fct type with the respective ratio of out-of-plane to in-plane unit cell dimensions  $c/a=1.38$ , and  $c/a=1.22$ , in agreement with the expectations for tetragonally distorted fcc Fe states.<sup>26</sup> Accordingly, the height of one atomic layer of  $\pi$  or  $\gamma$  phase is respectively  $h_\pi=1.83$  Å or  $h_\gamma=1.68$  Å.

The nucleation of the  $\gamma$  phases into the pseudomorphic phase for as-deposited films takes place by formation of  $\gamma$ -like patches with somehow irregular distribution.<sup>15</sup> The two phases likely tend to occupy neighboring patches in the film that can extend vertically for a few layers, similar to other metal-on-metal heteroepitaxial structures.<sup>27</sup> At some critical thickness, the  $\gamma$  patches will eventually coalesce, and all the topmost layers of the film will be in  $\gamma$  phase.

After the annealing, for films thinner than 9.5 Å, the combined analysis of diffraction patterns and AES data suggests the formation of Fe mounds with a mean size of about 10 nm. This interpretation is supported by the magnetic data also. The observation of tails of magnetization above  $T_C$  (see Sec. III B) is, in fact, the signature of finite size effects ascribable to the presence of the mounds. On the other hand, the full remanence of the MOKE hysteresis loops in the annealed state indicates that the mounds are separated by thin interstitial regions but remain *well connected*.<sup>22</sup> The large increase of the  $\pi$  peak intensity in the spot profiles, and the corresponding decrease of the  $\gamma$  contribution after the annealing are due to two superimposing effects. First, it reflects some possible substrate contribution to the LEED pseudomorphic peak, second the modification of the strain within the film due to the formation of mounds might favor the enduring presence of the  $\pi$  phase at the expense of  $\gamma$ .

For thicknesses larger than 9.5 Å, we simply observe a slight increase of the amount of Au interdiffused or segregated within the film. The presence of Au impurities can in turn help to stabilize the  $\pi$  phase,<sup>5</sup> at the expense of  $\gamma$ . This justifies the increase of the relative weight of the  $\pi$  phase with respect to the  $\gamma$  phase also observed for thickness larger than 9.5 Å.

### B. Magnetism

Our goal is to determine whether the two Fe phases co-existing in the film possess different magnetic properties.

The first clear evidence that emerges from our data is that both  $\pi$  and  $\gamma$  phases are FM ordered. However, other differences may exist; for example the different lattice constant and tetragonal distortion are expected to induce a different magnetic moment per atom.<sup>12,13</sup>

Rather than having access to the magnetic moment, MOKE has access to the magneto-optical coupling constant. In order to determine an eventual difference in the magneto-optical coupling constant, we have fitted with a straight line the thickness dependence of the  $A_K(0)$  for the as-deposited films (in the 7–14 Å range) and the annealed films (above 10 Å). The fits are reported as solid lines in the top panel of Fig. 5. For the as-deposited films the value of  $A_K(0)$  extrapolated to zero thickness yields a value of the intercept of  $4 \times 10^{-4} \pm 6 \times 10^{-4}$ , compatible with zero. For the annealed films, the slope of the linear fit to  $A_K(0)$  is compatible with the one for as-deposited data, and the intercept is negative ( $-1.3 \times 10^3 \pm 0.1 \times 10^{-3}$ ). Therefore the as-deposited films are uniformly magnetized and no differences between the magneto-optical response of the  $\pi$  and  $\gamma$  can be resolved. The negative intercept of the annealed films can be interpreted in terms of the formation of an interfacial dead magnetic layer due to substrate atom interdiffusion. The effective thickness of such a dead layer is constant with film thickness and can be estimated from the value of the intercept as 1.5 Å. The behavior of  $A_K(0)$  after annealing for thicknesses below 9.5 Å might be related to the influence of the mounds on the magnitude of the Kerr signal.

The thickness dependence of the Curie temperature  $T_C$  for both as-deposited and annealed film is interesting. The Curie temperature of ultrathin magnetic films is typically found to be lower than the bulk value, due to finite size effects.<sup>28</sup> For many film systems a scaling relation between the Curie temperature and the film thickness holds,<sup>29</sup> while in other cases, morphological and structural effects strongly affect this otherwise regular behavior.<sup>30–33</sup>

We focus our attention on the as-deposited films first. Looking at the thickness dependence of  $T_C$ , we notice that two thickness regions characterized by different properties are present, as pointed out in Sec. III B. The first such region extends from 7 to 12 Å thickness. It is characterized by a very weak thickness dependence of  $T_C$ , and by large irreversibility upon annealing.

For thicknesses larger than 12 Å,  $T_C$  increases more rapidly, and almost no irreversibility occurs upon annealing. At this point we notice that the films within the thickness range 9–13 Å are all subject to a temperature induced structural phase transition, referred to as reversible breakdown of pseudomorphism,<sup>8</sup> that reversibly modifies the film structure. Its critical temperature is thickness dependent and increases from 345 K (9 Å) to 380 K (13 Å). We can assume that the irreversible modifications in the as-deposited films start to take place around the critical temperature of the reversible breakdown of pseudomorphism. However, the thickness dependence of  $T_C$  cannot be due to the influence of the reversible breakdown of pseudomorphism because the Curie temperature is systematically lower than the critical temperature of the structural phase transition.

In order to account for our observation we propose the following model. In the thickness region between 7 and 11.4

Å the magnetism of the film, despite the simultaneous presence of  $\pi$  and  $\gamma$ , is driven by the topologically connected  $\pi$  phase. In this stage, we model the  $\gamma$  phase as made of patches that are not interconnected, similar to what is observed for other metal-on-metal heteroepitaxial systems.<sup>27</sup> We recall that the  $\gamma$  phase has larger relative weight in the LEED profiles due to the limited electron sampling depth. Therefore, in order to establish long range magnetic order, the exchange coupling within the  $\pi$  phase is the crucial quantity. As long as the  $\pi$  phase is FM ordered, also the independent and disconnected  $\gamma$  patches are kept FM aligned. As soon as the temperature destroys the FM order in the  $\pi$  phase, the long range order is lost. The atoms belonging to the  $\gamma$  phase might still be ferromagnetically aligned within each single patch, however, the alignment between the patches is lost.

When the patches of the  $\gamma$  phase become connected, the exchange coupling can be sustained also directly via the  $\gamma$  phase atoms at gradually higher temperatures. Experimentally, at this stage the Curie temperature starts to increase more steeply, prompting the conclusion that the strength of the exchange interaction pertinent to the  $\gamma$  phase is stronger than the one of  $\pi$ . At a thickness of 12.5–13.5 Å we are witnessing the initial stages of this process, as the rise of  $T_C$  eventually becomes even steeper at larger thickness. We again stress that our LEED data do not show the onset of a bcc-like phase up to 14.5 Å thickness.

Moving to the annealed films, we can trace the effect of the modifications in the structure and the morphology on the Curie temperature. We clearly observe a decrease of  $T_C$  which depends on the film thickness. Since the Fe mounds formed upon annealing remain connected, superparamagnetism should not play any role. Instead, for a system of well connected islands the long range FM order may be weakened due to the thinning of the interstitial regions between the mounds that are fundamental in keeping the various islands ferromagnetically aligned, thus accounting for the decrease in  $T_C$  after annealing. Clearly, an increase in the film thickness leads to a larger thickness of the interisland connection, thereby accounting for the observed increase of  $T_C$  with thickness. Alternatively it has been suggested<sup>31</sup> that the annealing can modify the strain distribution in thin films. This in turn can modify the magnetic anisotropy, a crucial quantity in determining the Curie temperature, and eventually lead to a lowered  $T_C$ .

In the highest part of the investigated thickness range, the main effect of the annealing is a change in the relative weight of the  $\pi$  and  $\gamma$  phases, likely driven by a rearrangement of the  $\gamma$  patches that minimizes the strain. When the  $\gamma$  phase has become connected, the film is stable enough that the annealing at 395 K is not sufficient to induce any major modification, thereby leaving the Curie temperature almost unchanged.

The temperature dependence of the magnetization in the thickness range for which the  $\gamma$  phase coalesces unlikely obeys the scaling relation of Eq. (1). The attempt to fit this behavior to the scaling relation therefore yields to the previously mentioned high values for  $\beta$ . Rigorously speaking, the Curie temperature itself cannot be determined in principle by the procedure that we employ. However, this applies only to

thicknesses greater than 12 Å and introduces a limited uncertainty that does not affect the core of our results.

## V. CONCLUSION

In conclusion, we have reported a study of the correlation between magnetism and structure of fcc-like Fe films grown on Cu<sub>3</sub>Au(001). We have shown that the coexistence of two fct structural phases in the same film affects the magnetic properties of the films. The two phases are, respectively, pseudomorphic to the substrate ( $\pi$ ), or have partly decreased the compressive strain by enlarging the in-plane lattice spacing ( $\gamma$ ).

No resolvable difference between the magneto-optical coupling constant between the two phases has been found. Instead, we have deduced from the correlation between the

thickness dependence of the film structure and of the Curie temperature that the  $\pi$  phase is characterized by a lower value of exchange coupling with respect to  $\gamma$ . We suggest that the similar values of the magneto-optical coupling constant between the two phases is due to their similar atomic volume, while the differences in the exchange coupling are due to modified geometry of the local atomic environment. We believe that the comprehensive structural and magnetic data now available for the Fe/Cu<sub>3</sub>Au(001) system can make it appealing for the verification of the calculated properties of Fe in fct state.

The authors thank Luca Floreano for a critical reading of the manuscript. Financial support from the MIUR-FIRB Program No. RBNE01XSW and MIUR-PRIN Program No. 2004029329 is acknowledged.

\*Electronic address: Bisio@fisica.unige.it

- <sup>1</sup>R. Rochow, C. Carbone, T. Dodt, F. P. Johnen, and E. Kisker, *Phys. Rev. B* **41**, 3426 (1990).
- <sup>2</sup>M.-T. Lin, J. Shen, W. Kuch, H. Jenniches, M. Klaua, C. M. Schneider, and J. Kirschner, *Phys. Rev. B* **55**, 5886 (1997).
- <sup>3</sup>B. Feldmann, B. Schirmer, A. Sokoll, and M. Wuttig, *Phys. Rev. B* **57**, 1014 (1998).
- <sup>4</sup>B. Schirmer, B. Feldmann, and M. Wuttig, *Phys. Rev. B* **58**, 4984 (1998).
- <sup>5</sup>F. Bruno, S. Terreni, L. Floreano, A. Cossaro, D. Cvetko, P. Luches, L. Mattera, A. Morgante, R. Moroni, M. Repetto, A. Verdini, and M. Canepa, *Phys. Rev. B* **66**, 045402 (2002).
- <sup>6</sup>F. Baudelet, M. T. Lin, W. Kuch, K. Meinel, B. Choi, C. M. Schneider, and J. Kirschner, *Phys. Rev. B* **51**, 12563 (1995).
- <sup>7</sup>M. Canepa, P. Cantini, C. Mannori, S. Terreni, and L. Mattera, *Phys. Rev. B* **62**, 13121 (2000).
- <sup>8</sup>F. Bisio, S. Terreni, G. Gonella, L. Floreano, A. Morgante, M. Canepa, and L. Mattera, *Phys. Rev. Lett.* **93**, 106103 (2004).
- <sup>9</sup>D. Tillmann and E. Kisker, *Solid State Commun.* **100**, 415 (1996).
- <sup>10</sup>A. Verdini, L. Floreano, F. Bruno, D. Cvetko, A. Morgante, F. Bisio, S. Terreni, and M. Canepa, *Phys. Rev. B* **65**, 233403 (2002).
- <sup>11</sup>V. L. Moruzzi, P. M. Marcus, K. Schwarz, and P. Mohn, *Phys. Rev. B* **34**, 1784 (1986).
- <sup>12</sup>V. L. Moruzzi, P. M. Marcus, and J. Kübler, *Phys. Rev. B* **39**, 6957 (1989).
- <sup>13</sup>P. M. Marcus, V. L. Moruzzi, and S. L. Qiu, *Phys. Rev. B* **60**, 369 (1999).
- <sup>14</sup>A. Biedermann, R. Tscheliessnig, M. Schmid, and P. Varga, *Phys. Rev. Lett.* **87**, 086103 (2001).
- <sup>15</sup>M. T. Lin, J. Shen, W. Kuch, H. Jenniches, M. Klaua, C. M. Schneider, and J. Kirschner, *Surf. Sci.* **410**, 290 (1998).
- <sup>16</sup>S. Gallego, L. Szunyogh, P. Weinberger, and M. C. Munoz, *Phys. Rev. B* **69**, 224408 (2004).
- <sup>17</sup>F. Bisio, G. Gonella, M. Canepa, S. Terreni, and L. Mattera, *Appl. Surf. Sci.* **212**, 166 (2003).
- <sup>18</sup>C. Mannori, G. Boato, M. Canepa, P. Cantini, L. Mattera, and S. Terreni, *Europhys. Lett.* **45**, 686 (1999).
- <sup>19</sup>C. Mannori, T. Scimia, P. Cantini, S. Terreni, M. Canepa, and L. Mattera, *Surf. Sci.* **433**, 307 (1999).
- <sup>20</sup>S. Terreni, M. Canepa, L. Mattera, and V. A. Esaulov, *Nucl. Instrum. Methods Phys. Res. B* **193**, 550 (2002).
- <sup>21</sup>P. Luches, A. Di Bona, S. Valeri, and M. Canepa, *Surf. Sci.* **471**, 32 (2000).
- <sup>22</sup>C. Martinez Boubeta, C. Clavero, J. M. Garcia-Martin, G. Armelles, A. Cebollada, L. Balcells, J. L. Menendez, F. Peiró, A. Cornet, and M. F. Toney, *Phys. Rev. B* **71**, 014407 (2005).
- <sup>23</sup>A. di Bona, C. Giovanardi, and S. Valeri, *Surf. Sci.* **498**, 193 (2002).
- <sup>24</sup>W. Dürr, M. Taborelli, O. Paul, R. Germar, W. Gudat, D. Pescia, and M. Landolt, *Phys. Rev. Lett.* **62**, 206 (1989).
- <sup>25</sup>J. A. Stroschio, D. T. Pierce, M. D. Stiles, A. Zangwill, and L. M. Sander, *Phys. Rev. Lett.* **75**, 4246 (1995).
- <sup>26</sup>P. M. Marcus and F. Jona, *Surf. Rev. Lett.* **1**, 15 (1994).
- <sup>27</sup>G. A. Rizzi, A. Cossaro, M. Petukhov, F. Sedona, G. Granozzi, F. Bruno, D. Cvetko, A. Morgante, and L. Floreano, *Phys. Rev. B* **70**, 045412 (2004).
- <sup>28</sup>M. Bander and D. L. Mills, *Phys. Rev. B* **38**, R12015 (1988).
- <sup>29</sup>F. Huang, M. T. Kief, G. J. Mankey, and R. F. Willis, *Phys. Rev. B* **49**, 3962 (1994).
- <sup>30</sup>J. Thomassen, F. May, B. Feldmann, M. Wuttig, and H. Ibach, *Phys. Rev. Lett.* **69**, 3831 (1992).
- <sup>31</sup>G. Garreau, M. Farle, E. Beaurepaire, and K. Baberschke, *Phys. Rev. B* **55**, 330 (1997).
- <sup>32</sup>U. Bovensiepen, P. Pouloupoulos, W. Platow, M. Farle, and K. Baberschke, *J. Magn. Magn. Mater.* **192**, L386 (1999).
- <sup>33</sup>P. Pouloupoulos, P. J. Jensen, A. Ney, J. Lindner, and K. Baberschke, *Phys. Rev. B* **65**, 064431 (2002).